COMPARISON OF DIFFERENT PROCEDURES FOR COMPUTING THE STRESS INTENSITY FACTOR RANGE FOR FATIGUE CRACK GROWTH TESTING AT 20 KHZ

Mohamed Sadek[1),*], Jens Bergström[1)] and Nils Hallbäck[1)]

[1)] Karlstad University, Department of Engineering and Physics, SE-658 88 Karlstad, Sweden

ABSTRACT

When computing the stress intensity factor (SIF) for high frequency loading it is important to consider dynamic effects such as inertia forces and damping. In the present study, different dynamic simulation procedures were carried out and the achieved SIF values were compared. Fast computation procedures such as modal analysis and direct steady-state analysis were compared to the computationally expensive transient dynamic analysis. Two different methods for calculating the SIF, the J-integral and the CTOD methods, were applied and compared and the results showed a near perfect agreement in calculation of the mode I SIF. The Rayleigh damping model was introduced into the dynamic computation to investigate its effect and the results revealed a clear effect on the SIF at 20 kHz frequency.

The fast direct steady-state analysis showed good agreement to both modal and transient analysis with the different damping values used and is recommended as the most effective procedure.

Keywords: *VHCF, stress intensity factor, transient analysis, modal analysis, direct steady-state analysis*

NOMENCLATURE

A	Crack area
a	Crack length
E_d	Dynamic elastic modulus
G	Shear modulus
ΔK	Stress intensity factor range
K_I	Mode I stress intensity factor
K_{II}	Mode II stress intensity factor
K_{III}	Mode III stress intensity factor
n_j	Unit vector
P	Work
r	Distance to the crack tip
T_i	Traction vector
U	Strain energy
U_0	Displacement at the top surface of the specimen
u	Displacement
u_0	Displacement magnitude
u_i	Displacement vector
u_x	Crack tip opening in mode II
u_y	Crack tip opening in mode I
u_z	Crack tip opening in mode III
w	Specimen width
α_R	Rayleigh damping mass-proportional coefficient
β_R	Rayleigh damping stiffness-proportional coefficient
ν	Poisson´s ratio
ρ	Material density
σ_{ij}	Stress tensor
ε_{ij}	Strain tensor
ω	Angular frequency
ξ	Rayleigh damping factor
Π	Potential energy

INTRODUCTION

In crack growth rate testing, usually the Paris law is used to define a crack growth curve. For that, a relation between the stress intensity factor range (ΔK) and the crack growth rate (da/dN) is required. While the crack growth rate is measured experimentally, the stress intensity factor (SIF) is computed analytically or numerically for a varying crack length. Crack growth testing using the ultrasonic fatigue testing system is carried out at 20 kHz load frequency, Fig. 1. A relationship between the controlling parameter of the testing system, i.e. displacement at the top of the specimen, and the mode I SIF at the crack tip in the mid-section of the specimen is required. In the present study, different computational methods were compared and a best practice is proposed.

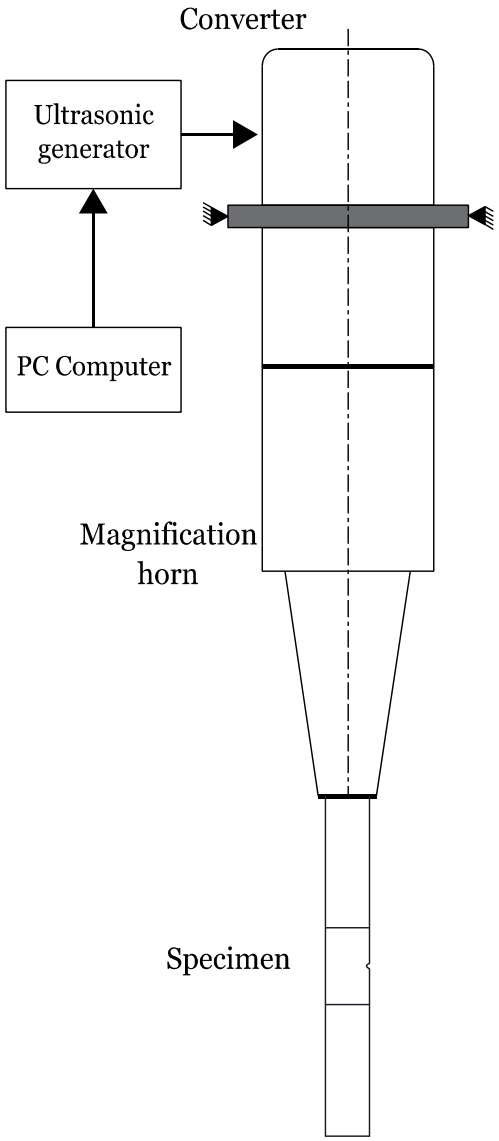

Fig. 1. Schematic figure displaying the main part of the ultrasonic fatigue testing system.

MODELLING AND COMPUTATION

There are different models for calculating the SIF. In elastic-plastic fracture mechanics, mainly two models are recommended, the J-integral and the Crack Tip Opening Displacement (CTOD)–methods [1, 2]. The J-integral method is based on the accumulated strain energy while the CTOD method is based on, namely, the crack tip opening displacements close to the crack tip.

When calculating the SIF for high frequencies, e.g. 20 kHz, static calculations are no longer enough. Inertia forces and damping effects are too significant to ignore at these high frequencies. Hence, dynamic analysis and simulations are highly recommended.

There are different computation procedures revealing the dynamic response of a system caused by harmonic excitation. Transient dynamic analysis, harmonic analysis and direct steady-state dynamic analysis are the different simulation procedures used and compared in this study.

Transient dynamic analysis

Discretisation of time yields a set of linear equations describing the response within each time increment. Such analysis starts with an unstable oscillation and converges to a steady oscillation. The time, or number of cycles required to pass the non-periodic transients and reach steady oscillation depends on material damping, with increased sensitivity at low damping coefficient [3]. The normalized SIF range variation during the first 20 simulated cycles is larger using smaller damping as demonstrated using three different values of damping, Fig. 2.

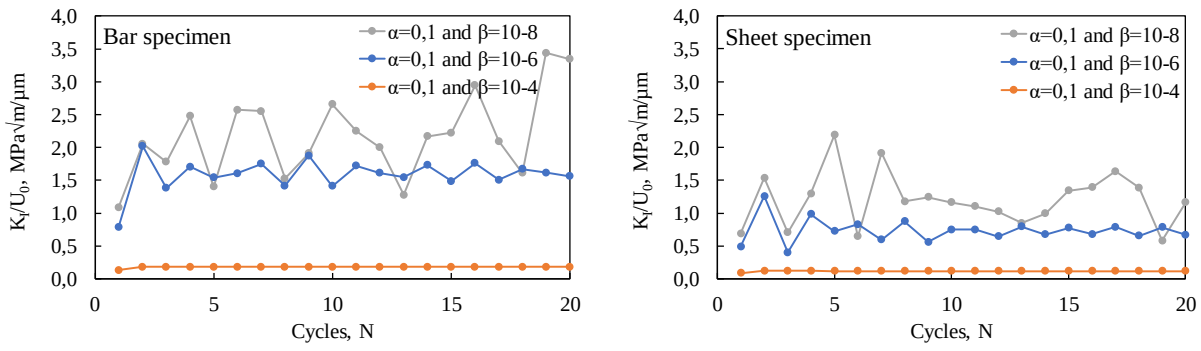

a) b)

Fig. 2. Normalized K_I during the first 20 cycles in transient dynamic analysis using three different values of the Rayleigh damping stiffness proportional coefficient. Calculated in the present study with a/w=0.29 and 20 kHz, for a) bar specimen, and b) sheet specimen.

In a previous study [4], a transient dynamic analysis has been described where the J-integral and thereby the SIF at a crack in a FCP bar specimen (Fig. 4a) has been computed. In [5-7] the same simulation procedure (transient dynamic) has been used to conduct stress-strain analysis in 20 kHz fatigue strength hour glass specimens. Such analysis is computationally expensive, especially when small values of material damping are used, and a large number of cycles is required to pass the transients and reach the steady state oscillation.

Harmonic modal analysis

While transient analysis is computationally expensive, harmonic modal analysis is a very cheap procedure. The analysis calculates the shape mode of the model at specific resonance frequencies in specific modes, i.e. modal analysis [2, 3, 8], and the computation procedure considers elastic material behaviour and does not take the damping into account. However, this simulation method can potentially eliminate large computational time consumption and hence is investigated in this study. The J-integral is not computed in a modal analysis hence the SIF is computed with the CTOD method. The simulation procedure has been used in some studies [9-12] to compute the SIF for crack growth rate analysis on some alloyed metals.

Direct steady-state dynamic analysis

Direct steady-state dynamic analysis is a linear perturbation procedure used to calculate the steady-state response of a system under a harmonic excitation at a prescribed range of frequencies. Conveniently, the frequency range is chosen to cover the desired resonance frequency computed in a preceded modal analysis (frequency extraction analysis). The response is calculated in terms of physical degrees of freedom using the mass, damping and stiffness matrixes. The commercial FEM software Abaqus offers two others, computationally cheaper, procedures for the calculation of the steady-state response; mode-based and subspace-based steady-state dynamics. However, the direct steady-state dynamic analysis is more accurate when frequency dependent damping (i.e. Rayleigh damping) is present [3].

The FEM software Abaqus yields the real part, imaginary part, magnitude and the phase angle of the solution. As in the transient analysis, when using damping, a phase shift exists in the oscillation of the model and increases as the distance to the region of the applied displacement

increases. In the direct steady-state analysis the phase shift is considered, and the maximum values are calculated according to Equation 1.

$$u = u_0 \cos(\omega t + \alpha) \quad [1]$$

where u_0 and α are the computed magnitude and phase angle, respectively, and ω is the angular frequency.

A direct steady-state method is explained in [13] where a simple model, Fig. 3, has been analysed. The steady-state solution of the same has also been computed by transient dynamic analysis and with a perfect match to the direct steady-state analysis.

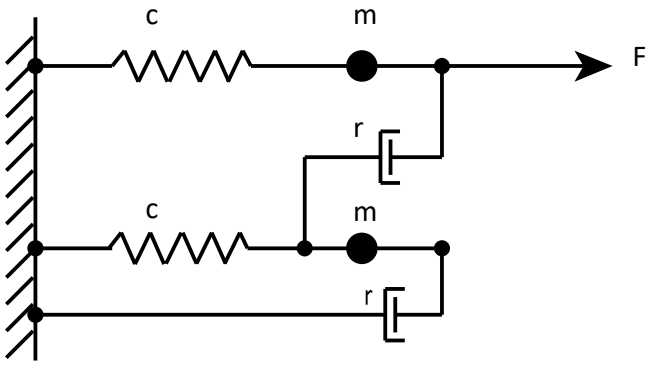

Fig. 3. Elastic-viscoplastic model with two mass points and a periodic force F=f(t).

Static analysis

In many instances, the stress intensity is calculated without taking into account the dynamic conditions, i.e. a static analysis is applied, for simplicity of the analysis. However, at higher load frequencies there are discrepancies needed to be recognized. In static simulations the load is ramped up to a chosen stress level and held constant. No oscillation is applied and the dynamic effects (inertia forces) are not considered [3]. In such analysis, the SIF can be calculated using both the J-integral and the CTOD methods.

Objectives

The objectives of the present study are to acquire more knowledge regarding the effects of specimen geometries (bar and sheet), methods of calculation (J-integral and CTOD) and simulation procedure on the stress intensity range ΔK. Furthermore, a best practice for computing the SIF at 20 kHz loading frequency is discussed.

MATERIALS AND SIMULATIONS CHARACTERISTICS

Two specimen geometries, bar and sheet, were considered in this study, Fig. 4. The mechanical characteristics used in the simulations are typical for steels: E_d=210 GPa, ν =0.3 and ρ=7800 kg/m^3. The Rayleigh damping model, Equation 2, is implemented in the FEM software Abaqus and was conveniently used in all simulations [14].

$$\xi = \frac{\alpha_R}{2\omega} + \frac{\beta_R \omega}{2} \quad [2]$$

where ω is the angular frequency and α_R and β_R are the mass- and stiffness proportional damping coefficients, respectively. At high frequencies (e.g. 20 kHz), the mass proportional damping is insignificant, and the stiffness proportional damping becomes the dominant part of the Rayleigh damping.

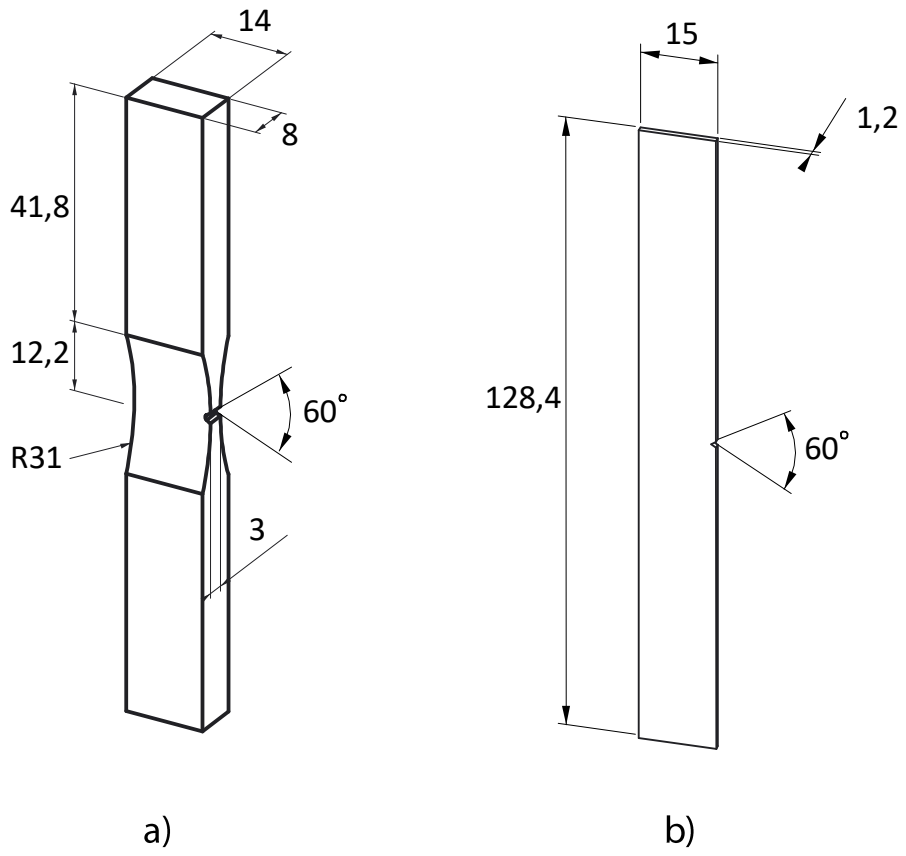

Fig. 4. 20 kHz FCP specimen: a) bar specimen and b) sheet specimen.

When using complicated specimen geometry (i.e. varying cross-sections, notches etc.) FEM software are conveniently used in particular when including the dynamic effects into the calculations. In this study, the FEM software Abaqus was used to compute the SIF for the two different specimen geometries using both the J-integral and CTOD methods.

For the simulations a ½ symmetry 3D-model was used for both specimen geometries, and the horn was included, see Fig. 5. As mentioned earlier, a previous study [4] has presented a best practice method where the whole load train has been included (specimen, horn and oscillator) into the simulated 3D-model. However, for the sake of minimizing the number of degrees of freedom, the oscillator was removed from the present simulation procedure as it is a comparative study.

A hexagonal focused mesh around the crack tip (Fig. 6) and a tetrahedral mesh for the rest of the model was used in all simulations. Two different sets of crack lengths were chosen for the two specimen geometries to be simulated for every variation in the simulation model.

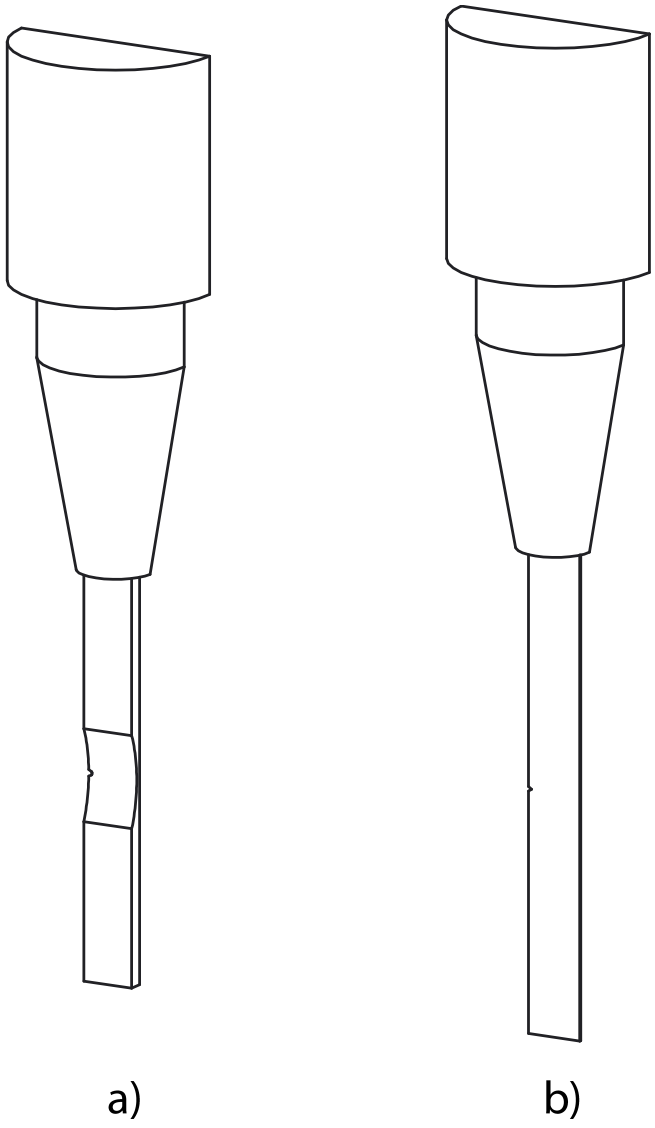

Fig. 5. The ½ symmetry 3D-models of the a) bar, and b) sheet specimens, and including the horn.

The focused mesh around the crack tip contains 8 contours. The 8 nodes on the crack lip, at the middle in the thickness direction and at the 8 contours, Fig. 6, were used to extract both the J-integral values and the displacement values used in the CTOD method.

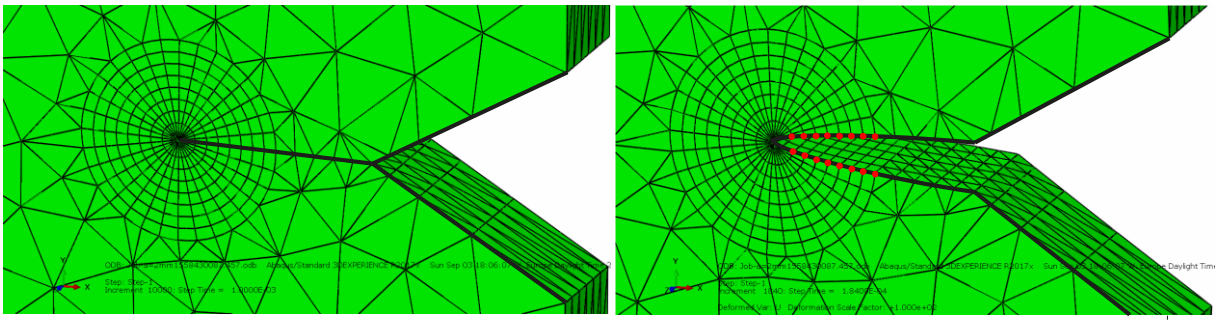

a) b)

Fig. 6. Focused hexagonal mesh around the crack tip containing 8 contours, a) closed, and b) open crack in the sheet specimen.

In the transient analysis, a harmonic excitation was applied as a sinusoidal displacement (u=4µm) to the top surface of the horn at the chosen frequency. The horn has a magnification factor of 2½ increasing the sinusoidal displacement to approximately u=10µm at the top of the specimen.

The simulations were run for 0.001 seconds enough for 20 cycles. Physical, elastic and damping properties were input to the analysis. The SIF in all three modes (K_I, K_{II} and K_{III}) were automatically computed by Abaqus using the J-integral method. For the CTOD method however, the displacements in all three directions (u_x, u_y and u_z) at the eight mentioned nodes (red nodes in Fig. 6) were plotted and used to calculate and extrapolate K_I, K_{II} and K_{III} at the crack tip, as in Fig. 8.

For the modal analysis, only physical and elastic properties were used since the damping is not considered in such analysis. The outcome of this analysis is the modal shape of the system, including horn and oscillator, at the found resonance frequency. The modal shape reveals the normalized displacement of all nodes in the model. The displacements at the specimen top surface and the nodes at the crack lips are extracted and used to compute the SIF with the CTOD method.

The direct steady-state dynamic analysis requires, as the transient analysis does, physical, elastic and damping properties. The range of frequency was specified to cover the desired frequency, and a displacement amplitude was applied to the horn top surface, u=4µm. The results of this analysis reveal, similarly to the modal analysis, the displacements of all nodes in the model including the CTOD´s.

The resonance frequency of the system will decrease as the crack length increases due to change in specimen compliance. For the direct steady-state analysis, the crack length specific harmonic modal frequency was used. For the transient dynamic analysis, both the harmonic modal frequencies and experimentally measured frequencies at the individual crack lengths were used. For the bar specimen, the experimental frequencies were measured in the present study while the experimental frequencies for the sheet specimen were provided by collaborative researchers at Université Paris Ouest (UPO) [12].

COMPUTATION OF THE STRESS INTENSITY FACTOR

The SIF for a varying crack length is achieved by interpolation of computed K_I for several specific crack lengths. In [4], in relation to static simulation, a clear increase in the computed K_I was shown when using a dynamic simulation including the frequency and damping effect.

For elastic-plastic materials with non-linear material deformation in a large region around the crack tip, the Linear Elastic Fracture Mechanics (LEFM) is no longer valid. Hence the development of an alternative model, the Elastic-Plastic Fracture Mechanics (EPFM) model, taking the plastic deformation into account [1]. The J-integral and the CTOD are two parameters describing crack tip conditions in elastic-plastic materials.

The experimental testing at 20 kHz with the ultrasonic fatigue system is a displacement controlled testing procedure run according to Equation 3. The displacement of the top surface of the specimen (U_0) is the controlled amplitude during testing [2].

$$K_I = \frac{E_d}{1-\nu^2}\, U_0 \sqrt{\frac{\pi}{a}}\, f(a/w) \qquad [3]$$

where E_d and ν are the elastic Young´s modulus and Poisson's ratio, respectively. a is the crack length and the function f(a/w) is the dimensionless shape function to be calibrated. From Equation 3 it is seen that the effects of U_0, E_d and ν on the SIF are simple and clear. However, there are more material properties involved in this computation, e.g. density and damping. These two properties are embedded in the shape function, f(a/w).

For the sake of comparison, the computed K_I in Fig, 9-11 with the different simulation procedures are all corresponding to when U_0=1 µm.

Calculating ΔK using the J-integral method

The J-integral is equivalent to the energy release rate in a body containing a crack. It relates the change in the potential energy to the crack growth, Equation 4 [1].

$$J = -\frac{d\Pi}{dA} \quad [4]$$

where A is the crack area and Π is the potential energy defined as:

$$\Pi = U - P \quad [5]$$

where U is the strain energy and P is the work done by external forces.

The J-integral for an arbitrary counter-clockwise path Γ around the crack tip is written as:

$$J = \int_{\Gamma} \left(W\, dy - T_i \frac{\partial u_i}{\partial x}\, ds \right) \quad [6]$$

where W is the strain energy density given by:

$$W = \int_0^{\varepsilon_{ij}} \sigma_{ij} d\varepsilon_{ij} \quad [7]$$

where σ_{ij} and ε_{ij} are the stress and strain tensors, respectively. T_i (Equation 8) and u_i are the components of the traction vector and the displacement vector, respectively, and ds is a length increment along the path Γ.

$$T_i = \sigma_{ij} n_j \quad [8]$$

where n_j are the components of the unit vector normal to the path Γ.

The SIF´s are extracted from the computed J-integral with Equation 9:

$$J = \frac{1}{8\pi} \overline{K}^T * \bar{B}^{-1} * \overline{K} \quad [9]$$

where

$$\overline{K} = [K_I, K_{II}, K_{III}]^T \quad [10]$$

and $\overline{B}$ is the pre-logarithmic energy factor matrix, the diagonal for homogeneous and isotropic materials [3].

Calculating ΔK using the CTOD-method

The crack tip blunting is assumed proportional to the fracture toughness of the material and hence it can be estimated by the measurement of the displacement of the crack surfaces, i.e. the CTOD-parameter, see Fig. 7. The SIF´s in mode I, mode II and mode III fracture at the crack lip at a distance r from the crack tip are computed according to Equations 11-13 [1].

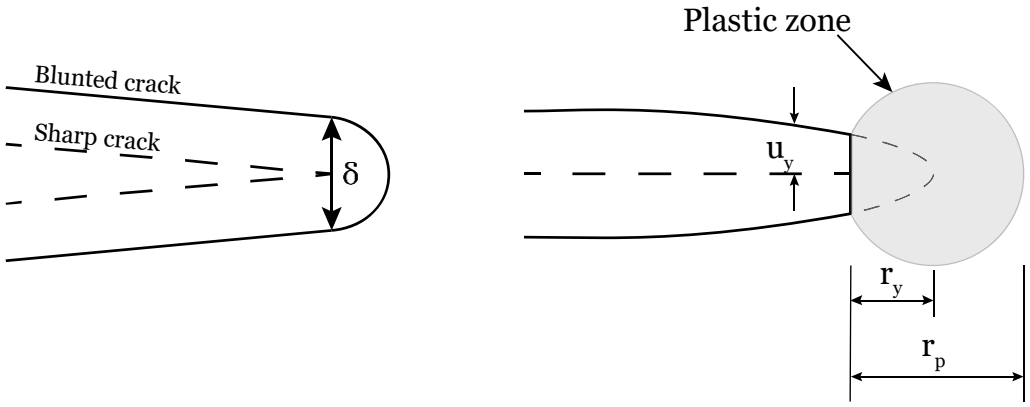

Fig. 7. Crack tip opening with a) crack tip blunting, and b) the effective crack length including the Irwin plastic zone correction [1].

$$u_y = \frac{\kappa+1}{2G} K_I \sqrt{\frac{r}{2\pi}} \quad [11]$$

$$u_x = \frac{\kappa+1}{2G} K_{II} \sqrt{\frac{r}{2\pi}} \quad [12]$$

$$u_z = \frac{2}{G} K_{III} \sqrt{\frac{r}{2\pi}} \quad [13]$$

where G is the shear modulus and $\kappa = (3\text{-}4\nu)$ for plane strain and 3D-models [1].

The CTOD´s (u_y, u_x and u_z) are measured at several positions near the crack tip and the SIF ´s at the crack tip are estimated by linear extrapolation, as illustrated in Fig. 8.

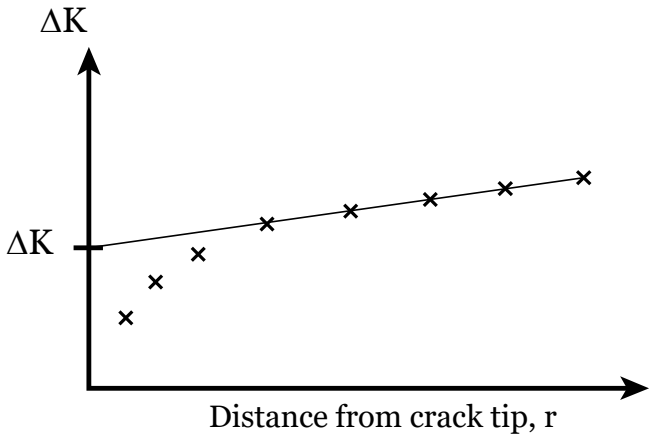

Fig. 8. Linear extrapolation of computed ΔK [12, 15].

RESULTS

Multiple series of simulations using the different simulation procedures, computation methods and frequencies were conducted on both specimen geometries. The results show a clear agreement between the two different computation models, the J-integral and the CTOD. Both the K_I by the J-integral and K_I by the CTOD method are acquired from the exact same simulations. Transient dynamic analysis was performed using experimental frequencies measured at each actual crack length, and where the experimental frequency decreases, from 20 kHz to 19.5 kHz, with advancing crack length due to loss in specimen stiffness. Then, the stress intensity in the bar specimen increases significantly with crack length a/w, while in the sheet specimen the increase is not as large, Fig. 9. All the same, the stress intensities computed by J-integral and CTOD methods agree perfectly.

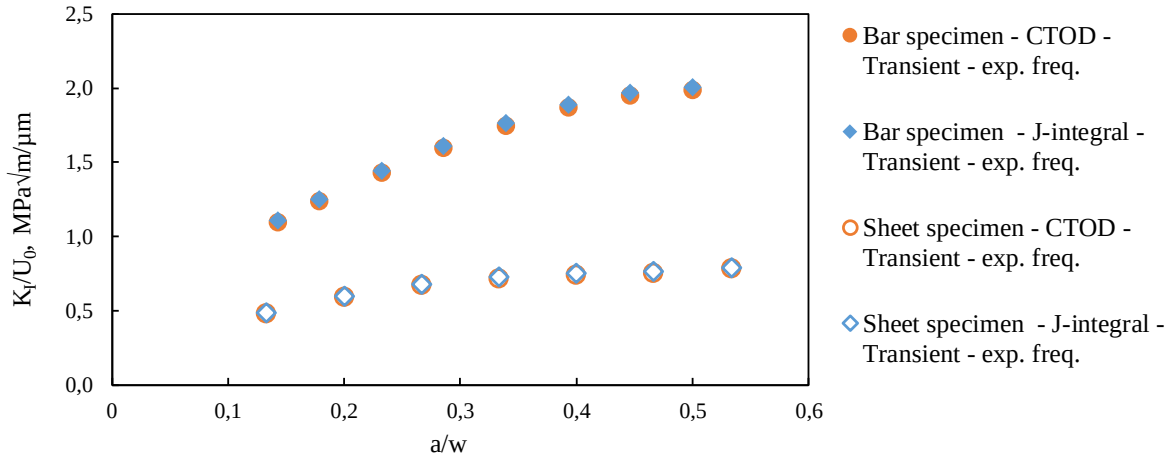

294

295 *Fig. 9. K_I-values corresponding to U_0=1µm plotted against a/w (where a is the crack length*
296 *and w is the specimen width) using J-integral and CTOD methods and bar and sheet*
297 *specimen geometries. Transient dynamic analysis and damping values α_R=0.1 and β_R=10^{-6}*
298 *was used.*

299

300 The static analysis results in significantly lower stress intensities than the dynamic analysis,
301 Fig. 10. However, the agreement between the J-integral and the CTOD methods was found
302 even when computing by static simulations, as shown in Fig. 10.

303

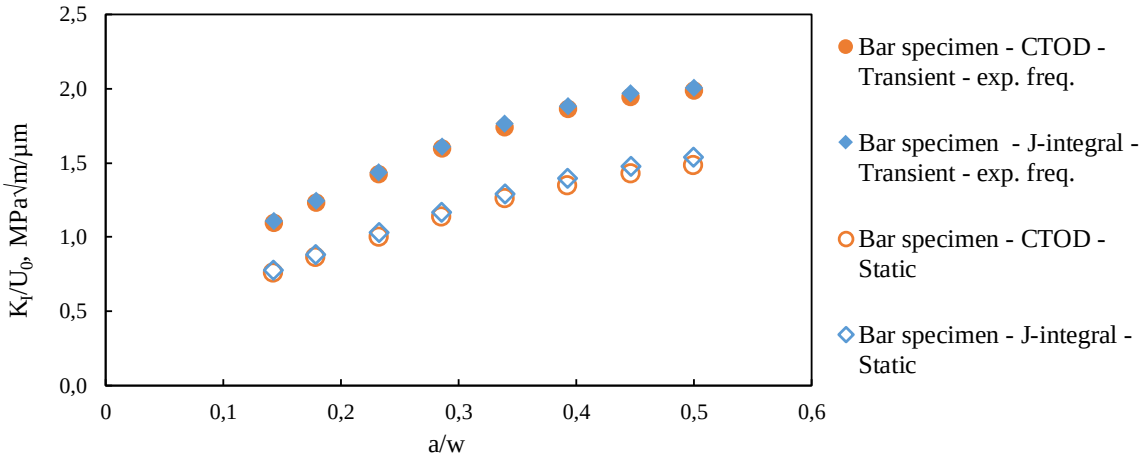

304

305 *Fig. 10. K_I-values corresponding to U_0=1µm plotted against a/w (where a is the crack length*
306 *and w is the specimen width) using J-integral and CTOD methods in static and transient*
307 *dynamic analysis of the bar specimen. Damping values α_R=0.1 and β_R=10^{-6} was used for the*
308 *transient dynamic analysis.*

Regarding the difference between the static and transient dynamic analysis, it is in agreement with results achieved in previous work [4] using the J-integral method where the static simulations showed K_I-values approximately 30% lower than dynamic transient simulations. In this work the same was computed with the CTOD method and the agreement between the two methods is again clear.

The results showed a clear difference between the SIF´s computed with transient dynamic analysis with Rayleigh damping coefficients α_R=0.1 and β_R=10^{-6} and the SIF´s computed with undamped harmonic modal analysis, using the same 3D-model and boundary conditions. The two transient dynamic analysis using two different frequency sets, experimentally measured and harmonic frequencies obtained by harmonic modal analysis, showed near perfect agreement. The difference between the two types of analysis, undamped harmonic modal and damped transient dynamic analysis, had opposite effect on the two specimen types. The SIF´s from the modal analysis appears higher than from the transient analysis for the bar specimen but lower for the sheet specimen, Fig. 11.

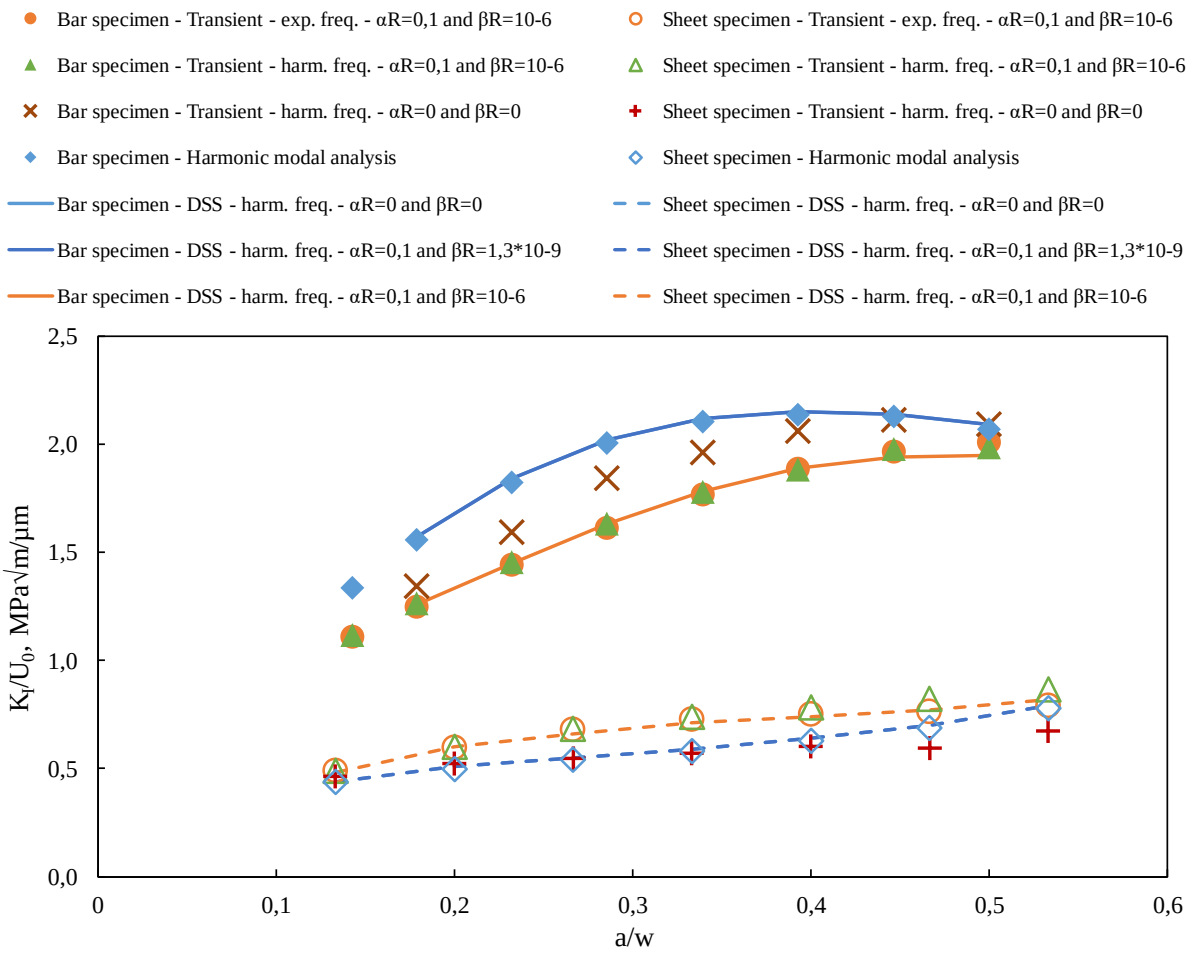

325

326 *Fig. 11. K_I-values corresponding to U_0=1µm plotted against a/w for bar and sheet specimens*
327 *computed by the CTOD method with transient, modal and direct steady-state (DSS) analysis*
328 *with different damping values.*

329

330 The SIF´s were also computed using the direct steady-state simulation procedure. Here three
331 different values of damping were used, undamped (α_R=0 and β_R=0), an experimentally
332 measured value (α_R=0.1 and β_R=1.3*10^{-9}) and the same values as used in the transient
333 analysis (α_R=0.1 and β_R=10^{-6}). The effect of the small damping value (α_R=0.1 and β_R=1.3*10^{-}
334 ^{9}) proofed to be negligible as the computed K_I-values coincides with those computed with the
335 undamped (α_R=0 and β_R=0) analysis. The higher damping value (α_R=0.1 and β_R=10^{-6})
336 however, showed a clear effect and the computed K_I-values were in good agreement with
337 those from the transient analysis (with the same damping values).

338 The mixed mode SIF´s, corresponding to approximately 10µm specimen top displacement,
339 are plotted in Fig. 12. K_I, K_{II} and K_{III} are all computed with the two different methods, J-
340 integral and CTOD, for a series of crack lengths. The simulation procedure used was transient

dynamic analysis and Rayleigh damping coefficients α_R=0.1 and β_R=10^{-6}. The values computed using the J-integral method showed that for relatively short cracks (up to 20% of the specimen width) K_{II} and K_{III} were essentially non-existent. However, as the crack grows longer K_{II} and K_{III} starts to elevate to significantly high values (K_{III} to higher values than K_{II}).

The CTOD method showed identical results regarding the K_I and K_{II} values. However, since there is no displacement in the mode III direction (i.e. u_z = 0), the CTOD method (Equation 13) gives K_{III} = 0.

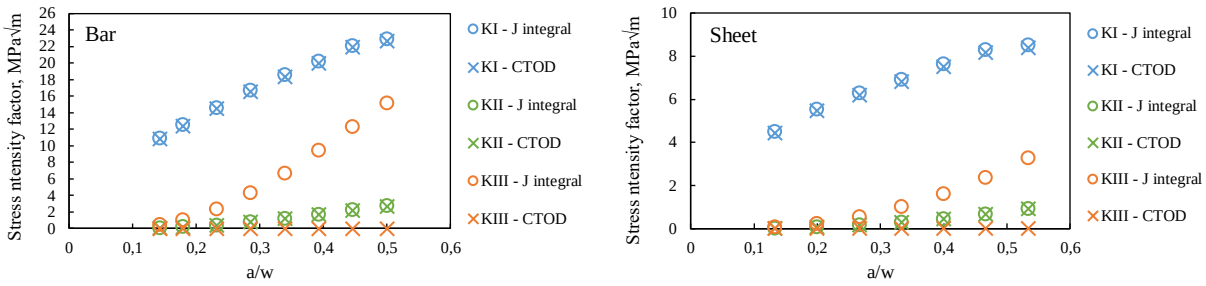

a) b)

Fig. 12. K_I, K_{II} and K_{III} computed with the two different methods, J-integral and CTOD using transient dynamic analysis with α_R=0.1 and β_R=10^{-6} and U_0=10µm. a) Bar and b) sheet specimen.

DISCUSSIONS

According to [1], elastic-plastic fracture mechanics (EPFM) is required when large plastic zone are surrounding the crack tip. Two different methods, the J-integral and the CTOD, are recommended for the computation of the SIF in elastic-plastic materials. Both models were used in this study and the results show a clear agreement between the two. The J-integral is more practical and is here recommended when using transient dynamic analysis since the SIF values are computed directly by the FEM software and are easily extracted. The CTOD-method is a bit more tedious to process. The displacements of the 16 crack lip nodes (red nodes in Fig. 6) are extracted and then extrapolated to calculate the SIF´s at the crack tip. However, it is not possible to acquire J-integral values from a modal or a direct steady-state analysis, hence the CTOD method is the recommended option when such simulation procedures are used.

The required fine mesh of the 3D-models used in this study yields a large number of degrees of freedom (DOF), $1\pm0.2*10^6$ DOF´s, and increases the computation effort for the simulations. Consequently, running transient dynamic analysis for more than 20 cycles in many series was considered too computationally expensive. It makes it difficult to extract qualitative results when using very small damping values, i.e. when the Rayleigh stiffness proportional damping coefficient $\beta_R<10^{-6}$. As shown in Fig. 2, the transient simulations reach a near steady-state oscillation during the first 20 cycles for $\beta_R\geq10^{-6}$ while for the $\beta_R=10^{-8}$ significant distortion is present throughout.

The average of the last 8 cycles (of 20 total) from $\beta_R=10^{-6}$ transient analysis is compared to the direct steady-state analysis with the same damping values, Fig. 11. The comparison shows good agreement for both specimen shapes. The $\beta_R=0$ and the $\beta_R=1.3*10^{-9}$ analysis are, as expected, in good agreement to the undamped modal analysis. The result of the modal analysis in this study were similar to results where the same analysis type and sheet specimen shape have been used [12].

Opposite to the bar specimen, the sheet specimen increased in K_I when $\beta_R=10^{-6}$ was used compared to when the lower $\beta_R=0$ or $\beta_R=1.3*10^{-9}$ damping values were used. However, it is clear that the $\beta_R=10^{-6}$ damping value effects the results, and that the effect varies with the crack length (i.e. a/w). A transient dynamic analysis with an undamped ($\alpha_R=0$ and $\beta_R=0$) specimen and damped horn ($\alpha_R=0.1$ and $\beta_R=10^{-6}$) was also carried out. The results from this analysis came closer to the modal and the undamped direct steady-state analysis. This confirms the effect of the damping on the computed K_I values, Fig. 11.

The comparison of K_I-values calculated with different damping values are based on finding the maximum K_I-values during one load cycle. But as damping introduces a phase shift, the maximum K_I-values will occur at different phase angles depending on the damping condition and increases with the distance from the applied displacement region. Therefore, the phase shift effect by damping was considered in both the transient and direct steady-state analyses and evaluation of the results. Examples and discussion on the matter follows below.

The applied harmonic displacement, the displacement at the specimen top and the K_I–value at the specimen mid-section crack tip, are displayed during cycle 20 of the transient analysis, Fig. 13. The evident phase shift in both specimen types, but the effect of the damping on the phase shift is more significant on the sheet specimen.

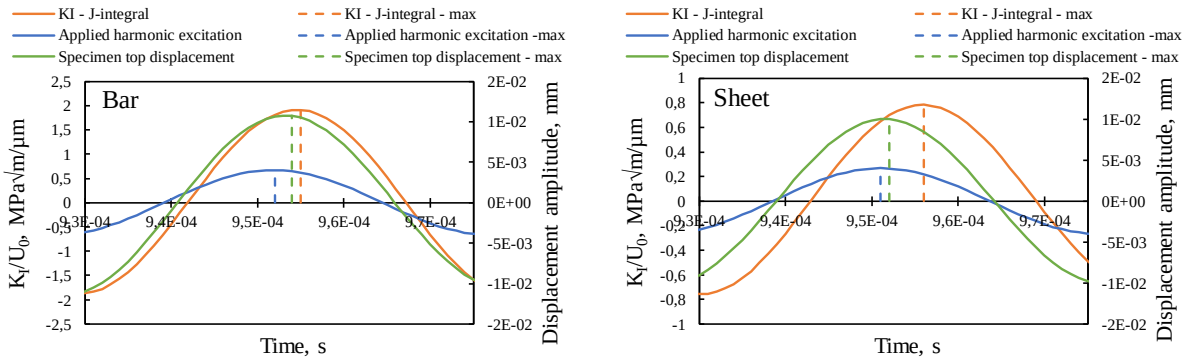

a) b)

Fig. 13. U_0, displacement of the top surface of the horn (i.e. applied harmonic displacement) and K_I corresponding to U_0=1µm plotted against time for a) bar and b) sheet specimen at (a/w=0.33). Transient dynamic analysis, J-integral method and $\beta_R=10^{-6}$ damping were used.

Thus, when extracting the relationship between the K_I and the specimen top displacement from the transient analysis, the maximum peak value is used from both the K_I and specimen top displacement curves in Fig. 13.

In the direct steady-state analysis, however, it is a bit trickier to consider the phase shift. Here, the magnitude and the phase angle of the 8 pair of nodes at the crack lips close to the tip, i.e. red nodes in Fig. 6, are extracted from the FEM software to calculate the maximum values according to Equation 1. The distance between the upper and lower nodes is plotted according to Equation 14 for all 8 pairs.

$$u = u_{upper\ node} - u_{lower\ node}$$

$$= \{u_0 \cos(\omega t + \alpha)\}_{upper\ node} - \{u_0 \cos(\omega t + \alpha)\}_{lower\ node} \quad [14]$$

The maximum values of this distance (u/2 curves in Fig. 14) are extracted and used to calculate K_I by the CTOD-method at the 8 contours, and then extrapolate K_I to the crack tip according to Fig. 8. The maximum displacement value of the specimen top surface is also calculated, according to Equation 1, using the u_0 and α parameters determined from the analysis.

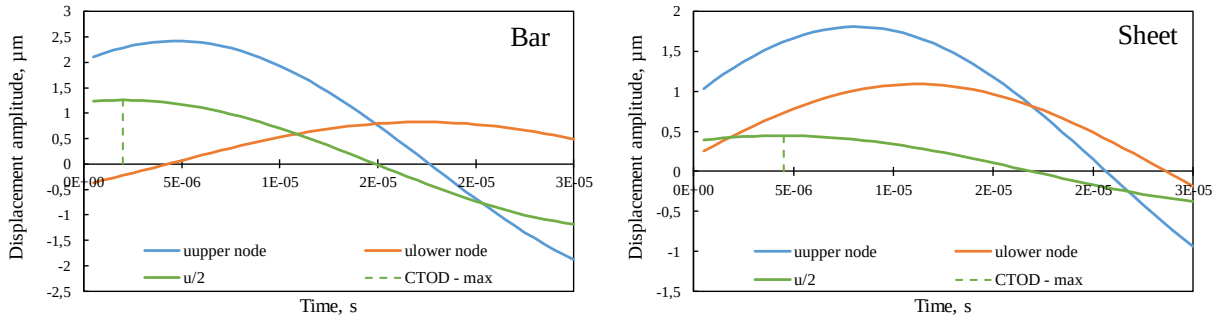

a) b)

Fig. 14. Displacements of upper and lower node of the first pair plotted together with distance between them according to Equation 14 for a) bar, and b) sheet specimen at a/w=0.33. Direct steady-state analysis, CTOD-method and $\beta_R=10^{-6}$ were used.

The results imply that when using the same argument during the evaluation of the results, the direct steady-state analysis yields the same results as a converged transient analysis. In the present study, the maximum K_I values were extracted and normalized against the maximum displacement value at the specimen top under the same cycle. The same procedure was carried out when evaluating the results from both transient and direct steady-state simulation procedures, hence the perfect match displayed in Fig. 11. A good agreement between the two different computation procedures have been proofed earlier for a very simple model of mechanical vibrations of the stator in an electrical machine [13]. The size of the model in the present study was scaled up and included a vast amount of DOF´s, still, two computation procedures are in good agreement.

The multi fracture mode analysis revealed partly expected and partly unexplainable results. The analysis mainly aimed to investigate the K_{II} and K_{III} computation by the two different computation methods, J-integral and CTOD. The computation of the mode I and mode II SIF´s yielded the same results using the two different methods, as seen in Fig. 12. In mode III SIF, however, the two methods ended up with mismatching results. Given the load mode and boundary conditions used, any crack tip opening displacements in the mode III direction are not expected. Consistent to this, it is confirmed by the CTOD method where the extracted u_z magnitudes (Equation 13) are zero. Contradictory, the J-integral method resulted in non-zero values of the K_{III}. In fact, they are significantly high, even higher than the K_{II}-values. The results are found questionable and yet to be explained. Hence, further investigation is required

on that the J-integral method yields non-zero K_{III} values, since this is an obvious anomaly here.

Finally, regarding the best practice for computing the SIF at 20 kHz loading frequency, the direct steady-state dynamic simulation procedure is recommended. A summary of K_I-values corresponding to U_0=1µm at a/w=0.33 computed with the different simulation procedures carried out in the present study, are presented in Table 1. Clearly, the direct steady-state analysis yields consistent results when comparing to the undamped modal and the damped transient analysis.

Table 1. Summary of K_I [MPa√m] values corresponding to U_0=1µm at a/w=0.33 computed with the different simulation procedures, and using the CTOD-method.

	Bar			Sheet		
	$\beta_R=0$	$\beta_R=1.3*10^{-9}$	$\beta_R=10^{-6}$	$\beta_R=0$	$\beta_R=1.3*10^{-9}$	$\beta_R=10^{-6}$
Modal analysis	2.1			0.58		
Transient analysis			1.78			0.74
Direct steady-state analysis	2.1	2.1	1.78	0.59	0.59	0.71

A best practice for computing the SIF at 20 kHz loading frequency was presented in a previous study [4], and proposed a transient dynamic analysis of the whole ultrasonic system load train (specimen, horn and oscillator) at the effective natural frequency ω_0, Equation 15, introduced by [16] taking into account the effect of a breathing crack on the eigenfrequency.

$$\omega_0 = \frac{2\omega_1\omega_2}{\omega_1+\omega_2} \qquad [15]$$

where ω_1 and ω_2 are the eigenfrequencies of an un-cracked and crack specimen, respectively.

Presently, the best practice is updated by recommending the direct steady-state dynamic analysis for the computation of the SIF, instead of the computationally expensive transient analysis. The remainder of the recommendations are the same.

As previously mentioned, the direct steady-state analysis does not include computation of the J-integral. Hence, the SIF computation performed with the CTOD-method proofed tedious

and time consuming during the work of this study. However, there is room for development of the computer software to improve the data evaluation process required for the CTOD-method.

CONCLUSIONS

The stress intensity factor for fatigue crack growth testing at 20 kHz loading frequency was successfully computed with several different simulation procedures; modal analysis, transient dynamic analysis and direct steady-state dynamic analysis. Furthermore, two different methods for evaluation of the stress intensity factor, J-integral and CTOD method, were used. An existing best practice for the stress intensity factor computation at 20 kHz was improved and the required computational cost was reduced significantly as of the results of this study.

- The two stress intensity computational methods, J-integral and CTOD, showed perfectly good agreement in computing the K_I in both specimen types and with different simulation procedures.
- Implementing damping into the dynamic simulations clearly affects the results. The effect is opposite in the two bar and sheet specimen types. A decrease in the computed K_I-value is noticed when using damping in the bar specimen and an increase in the sheet specimen.
- The different simulation procedures showed matching results with the different damping values used.
- The direct steady-state dynamic analysis procedure is hereinafter recommended as the most effective procedure computing the stress intensity factor at 20 kHz loading frequency with the damping taken into consideration.

ACKNOWLEDGEMENTS

The research leading to these results has received funding from the European Union's Research Fund for Coal and Steel (RFCS) research programme under grant agreement no. [RFS-CT-2013-00015 (FREQTIGUE)].

Acknowledgements to Mohand Ouarabi and Olivier Polit, Université Paris Ouest Nanterre La Defense (LEME) and Thierry Palin-Luc, Arts et Métiers Paris Tech, for providing experimental frequencies of sheet specimen.

AUTHOR´S CONRIBUTION

The major part of the planning, the computational work and the writing was carried out by the corresponding author Mohamed Sadek. The co-authors, Jens Bergström and Nils Hallbäck, contributed in the planning of the paper and the content of it, the evaluation of the results and the writing.

REFERENCES

1. Anderson, T.L. *Fracture Mechanics: Fundamentals and Applications*. 4th edition ed. Taylor & Francis, CRC Press; 2017.
2. Bathias, C. and Paris P.C. *Gigacycle fatigue in mechanical practice*. New York : Marcel Dekker; 2005.
3. Abaqus/CAE, *Abaqus Documentation*. 2019.
4. Sadek M, Bergström J, Hallbäck N, Burman C. Computation of and testing crack growth at 20 kHz load frequency. *Procedia Structural Integrity.* 2016;2: 1164-1172.
5. Tofique W.M., Bergström J, Hallbäck N, Burman C. Fatigue initiation and strength of duplex stainless steel strip specimens in the very high cycle fatigue regime. In: *6th International Conference on VHCF*. Chengdu, China. 2014.
6. Tofique, M.W., Bergström J, Svensson K, Very high cycle fatigue of cold rolled stainless steels, crack initiation and formation of the fine granular area. *International Journal of Fatigue.* 2017;100: 238-250.
7. Kazymyrovych V, *Very high cycle fatigue of tool steels*. Sweden: Karlstad University Press; 2010.
8. Mayer H.R., Stanzl-Tschegg S.E., Tan D.M.. FEM modelling of stress intensity factors for fatigue crack growth at ultrasonic frequencies. *Engineering fracture mechanics.* 1993;4: 487.
9. Ouarabi M, R.P.M., Bathias C, Palin-Luc T. Very high cycle fatigue strength and crack growth of thin steel sheets. *Frattura e Integrita Strutturale.* 2016;36: 7.
10. Palin-Luc T, Perez-Mora R, Bathias C, Dominguez G, Paris P.C, Arana J.L. Fatigue crack initiation and growth on a steel in the very high cycle regime with sea water corrosion. *Engineering Fracture Mechanics.* 2010;77(11): 1953-1962.
11. Tieying W., Bathias C. Application of fracture mechanics concepts in ultrasonic fatigue. *Engineering Fracture Mechanics.* 1994;47(5): 683-690.
12. Ouarabi M. Influense de la frequence de chargement sur la resistance a lámorcage et la croissance de fissure de fatigue dans des aciers utilises pour des applications mecaniques exigeantes. In: *Membre de lúniversite paris Lumiéres*. 2018: 242.
13. Rainer S, Biro O, Krischan K, Stermecki A, Philipp L. Direct steady-state computation of mechanical vibrations in electrical machines. In: *2008 18th International Conference on Electrical Machines*. 2008.
14. Cook R.D., Malkus D.S., Plesha M.E., *Concepts and applications of finite element analysis*. Wiley; 1989.
15. LE H.N., Etude de la propagation d'une fissure sous chargement thermique cyclique induisant un gradient de température dans l'épaisseur. In: *Sciences pour l'Ingénieur & Aéronautique*. ENSMA, Poitiers: 2009: 273.
16. Chati M., Rand R, Mukherjee S. MODAL ANALYSIS OF A CRACKED BEAM. *Journal of Sound and Vibration.* 1997;207(2): 249-270.